J Indian Soc Remote Sens (March 2018) 46(3):355–366
https://doi.org/10.1007/s12524-017-0679-5

RESEARCH ARTICLE

Atmospheric Correction Methods for GF-1 WFV1 Data in Hazy Weather

Zheng Wang[1,2,3] · Junshi Xia[4] · Lihui Wang[5] · Zhihua Mao[2,3] · Qun Zeng[6,7] · Liqiao Tian[8] · Liangliang Shi[9]

Received: 19 September 2016 / Accepted: 18 April 2017 / Published online: 14 July 2017

Abstract Increasing hazy weather in the eastern area of China limits the potential application of high-resolution satellite data and poses a huge challenge for the atmospheric correction of remote sensing images. Consequently, it is necessary to find the most suitable atmospheric correction method under hazy condition. In this study, five kinds of atmospheric correction models, including 6S, COST, FLAASH, QUAC, and ATCOR2, are applied to the GaoFen-1 Wild Field Camera (GF-1 WFV1) data in the eastern area of China, and examined by both quantitative and qualitative analyses using the measured spectrum data. Experimental results indicated that ATCOR2 achieves the best performance among the atmospheric correction methods qualitatively and quantitatively. Hence, specifically for the study area and GF-1 WFV1 dataset, ATCOR2 is the most suitable atmospheric correction approach under hazy in the eastern area of China.

Keywords Hazy · Atmospheric correction · GF-1 WFV1

✉ Zhihua Mao
mao@sio.org.cn

1 School of Geographic and Oceanographic Sciences, Nanjing University, Nanjing 210023, China

2 Collaborative Innovation Center for the South China Sea Studies, Nanjing University, Nanjing 210023, China

3 States Key Laboratory of Satellite Ocean Environment Dynamics, Second Institute of Oceanography, State Oceanic Administration, 36 Bochu North Road, Hangzhou 310012, China

4 Research Center for Advanced Science and Technology, The University of Tokyo, 4-6-1 Komaba, Meguro-ku, Tokyo 153-8904, Japan

5 Institute of Geodesy and Geophysics, Chinese Academy of Sciences, 340 XuDong Rd., Wuhan 430077, China

6 Editorial Department of Journal of Central China Normal University, Wuhan 430079, China

7 The College of Urban and Environmental Sciences, Central China Normal University, Wuhan 430079, China

8 State Key Laboratory of Information Engineering in Surveying, Mapping and Remote Sensing, Wuhan University, Wuhan 430079, China

9 Ocean College, Zhejiang University, 866 Yuhangtang Road, Hangzhou 310058, Zhejiang, China

Introduction

On April 26, 2013, China-made Gao-Fen (Gao-Fen in Chinese means high spatial resolution) (GF-1) was successfully launched. It is equipped with two 2-m panchromatic/8-m multi-spectral cameras, and four 16-m multi-spectral cameras (Wild Field Camera, or WFV). The scan width is 800 km with the repetition cycle of four days (Wu et al. 2015). Due to the large width multi-spectral data with high spatial and temporal resolutions, GF-1 can effectively avoid the conflict of traditional satellite spatial (temporal) resolution and width, and be widely used in land resource survey, environmental monitoring, precision agriculture, among others.

To achieve the application potentiality of GF-1 data, the premise is to obtain accurate surface information. However, the signals obtained by satellite sensors contain atmospheric water vapor, air molecules, aerosols, etc. The information of interest received by the sensor is only a small part of the total signals. When we apply these data to the aforementioned applications, the most important issue is to apply atmospheric correction first, to eliminate the effects of aerosols, water vapor and air molecules on radiative transfer, which is called atmospheric correction

(Gao et al. 2009). Atmospheric correction plays an important role in quantitative remote sensing. Atmospheric correction approaches mainly include: (a) image characteristics relative correction model, (b) ground-based linear regression model, (c) atmospheric radiative transfer model and complex models (Qi and Tian 2005). In recent years, many researchers investigated the performances of different atmospheric correction models on different spatial-resolution datasets. For instance, Richter (1996, 1997) proposed two atmospheric correction models, named Atmospheric and Topographic Correction model (ATCOR2) and ACTOR3 for medium spatial-resolution Landsat Thematic Mapper (TM) and SPOT High Resolution Visible (HRV) data. Liang et al. (2001, 2002) proposed an efficient method for Landsat Enhanced Thematic Mapper-Plus (ETM+) and validated it using measured data. Lu et al. (2002) used the Second Simulation of the Satellite Signal in the Solar Spectrum (6S) and Dark Object Subtraction (DOS) model for atmospheric correction of Landsat TM and applied them to real cases. Karpouzli and Malthus (2003) offered atmospheric correction for IKONOS data based on empirical linear model. Felde et al. (2003) applied Fast Line-of-sight Atmospheric Analysis of Spectral Hypercubes (FLAASH) atmospheric correction model to 30-m spatial resolution of Hyperion hyperspectral data. Matthew et al. (2003) also applied the FLAASH model to Airborne Visible Infrared Imaging Spectrometer (AVIRIS) hyperspectral data which is 20-m spatial resolution. Wu et al. (2005) carried out their study using the DOS-based model, Cosine Approximation Model (COST) and Apparent Reflectance (AR) model on QuickBird dataset in precision agriculture applications. Bernstein et al. (2005) used a quick atmospheric correction (QUAC) model for AVIRIS data and compared it with the results by the FLAASH model. Many methods were proposed for different sensors, such as DOS, 6S, QUAC, and FLAASH models for SPOT data (Wang et al. 2011; Guo and Zeng 2012; Han et al. 2012; Yang et al. 2015). FLAASH and ATCOR2 models were used for Landsat-TM/ETM (Yao et al. 2011). Look-up tables and 6S models were used for Quickbird data (Peng 2008), and 6S, FLAASH, COST, and QUAC models were used for Chinese HJ-charge-coupled device (HJ-CCD) data (Wang et al. 2014). The DOS and 6S models were applied to China Resources III (ZY-3), whose spatial resolution is 5.8 m (Guo 2014). According to our literature review, for the medium- and high-resolution data, the commonly used atmospheric correction models are 6S, COST, FLAASH, QUAC, and ATCOR2. As we know, relative atmospheric correction is statistically or empirically based atmospheric correction models, which use the input information from the image itself and do not rely on the evaluation of atmospheric components of any kind. Absolute atmospheric correction methods are physically based atmospheric correction methods, which require a detailed description of the components in the atmospheric profile. The new development of MODTRAN-based radiation transfer model was incorporated into the origin code of ATCOR2 and FLAASH to simulate the radiation transfer properties. MODTRAN, LOWTRAN and 6S model, which refer to the radiation transfer models, are all absolute atmospheric correction methods. COST and QUAC models are all relative atmospheric correction models.

The low visibility weather caused by haze, especially in the eastern area of China, has shown an increasing trend. Sustained hazy days present a huge challenge for atmospheric correction of satellite data. In order to achieve the advantages and potential of GF-1 data, it is necessary to verify 6S, COST, FLAASH, QUAC, and ATCOR2 models, and find out which method has excellent performance. Although GF-1 data were already been used for some applications, there is no study on atmospheric correction for GF-1 data (He et al. 2015). Therefore, the main purpose of this paper is to present a comparative study of atmospheric correction models on GF-1 WFV1 data using 6S, COST, FLAASH, QUAC, and ATCOR2 models. We will find an optimal model suitable for specific data and study area. Our results will promote the potential use of GF-1 WFV1 data and provide a reference for future studies using GF-1 WFV1 data.

Study Area and Data

Study Area

The study area is Fengqiu County (114°14′–114°46′E, 34°53′–35°14′N), Henan Province, which is located in the central North China Plain, with an altitude between 65 and 72.5 meters. It borders Yuanyang County and Yanjin County to the west, and Hua County and Changyuan County to the north. It is also next to the Yellow River, and across the river there are Lankao and Kaifeng counties. The area of Fengqiu County is 1220.5 km^2, covering about 0.68% of Henan Province. Figure 1 shows the composite false color image (GF-1) of the study area, and the yellow dots are the actual sites of the measured spectrum.

Data and Pre-processing

GF-1 is the first satellite of China High-resolution Earth Observation System (CHEOS) (Li et al. 2015). It is a break through against traditional high optical remote sensing technology, which combines high spatial resolution, multi-spectral and temporal resolution, multi-image mosaic load fusion, high precision and high stability of the attitude control technology. It has great significance in both theory

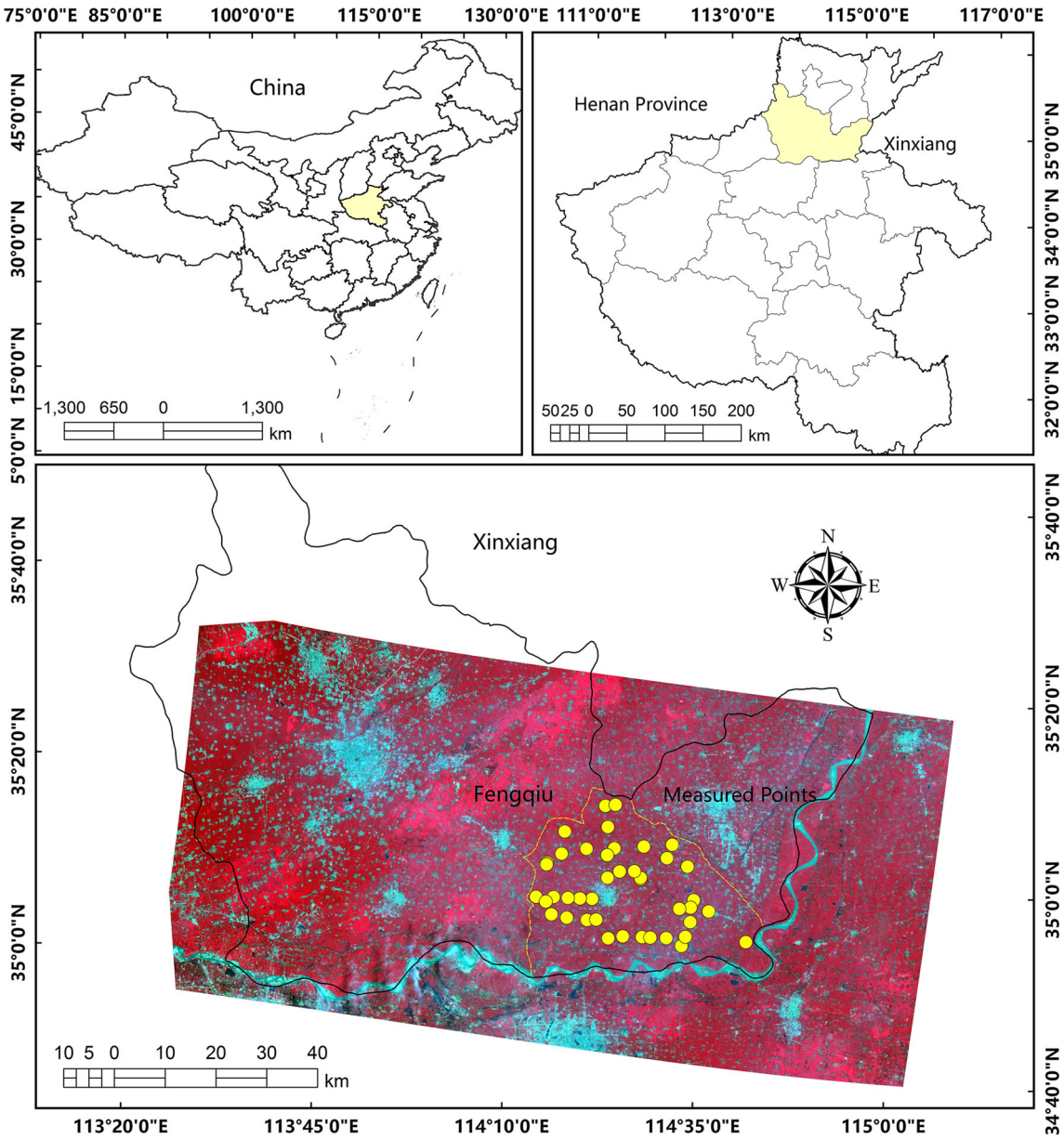

Fig. 1 Study area and the actual measurement sites (marked by *yellow dots*) (color figure online)

Table 1 The parameters of GF-1 WFV1. D is Sun-Earth distance, $ESUN_\lambda$ is the mean solar spectral irradiance of each band at the top of the atmosphere and θ is the solar zenith angle

Payload	Band	Spectral range (nm)	Gain	$ESUN_\lambda$	Other parameters	
WFV1	1	450–520	0.2004	1968.602	D	1.5×10^{11} m
	2	520–590	0.1648	1848.374	θ	63.62
	3	630–690	0.1243	1571.096	Resolution	16 m
	4	770–890	0.1563	1078.981	Recycled period	4 days

and applications. The parameters of 16-m multi-spectral camera GF-1 WFV1 are shown in Tab. 1.

Haze is formed by large size particles (mainly aerosol particles). The greater the particle size, the more light is scattered in the forward direction, which is described by the Mie's scattering model (Chavez 1988). In hazy condition, large size particles make nearly all the wavelengths of visible light scattered; that is why haze appears to be white or grey in the satellite image approximately (Fig. 1), and this is also the main reason leading to low visibility in

hazy days. To take advantages of GF-1 data and validate the performance of several atmospheric correction methods in hazy days, we choose the time when the value of aerosol optical thickness (AOD) is the highest. The North China Plain has the highest AOD in summer based on long-term time series of ground observations. Considering the haze process and many other factors, such as cloud cover, satellite signal and solar illumination conditions in August 2014, we select the GF-1 WFV1 data acquired on August 15, 2014 (sunny and cloudless) finally. The GF-1 WFV1 data acquisition date is corresponding to the actual measured data acquisition time in mid-August 2014.

In this work, the digital number (DN) values of GF-1 WFV1 image were first converted to radiance image according to the scaling factors named "Gain" in Table 1. Then, some kinds of atmospheric model based on radiative transfer and DOS model were used to convert radiance to reflectance. The top of the atmosphere reflectance (TOA), also known as the apparent reflectance without atmospheric correction, is the surface reflectance spectra at the top of the atmosphere, which was calculated by Eq. (1) below.

$$\rho_{TOA} = \pi * L_\lambda * D^2/(ESUN_\lambda * \cos(\theta)) \quad (1)$$

where L_λ is the radiance of each band after radiometric calibration.

Geometric correction should be applied to the GF-1 WFV1 image. Ground control points (GCPs) were obtained from Landsat 8 Operational Land Imager (OLI) data, which had been geometrically corrected, with a positional accuracy within 10 m. The chosen Landsat 8 OLI data, covering the same area as GF-1 WFV1, was resampled to the 16-m spatial resolution corresponding to GF-1 WFV1. A quadratic polynomial transformation was used to rectify the GF-1 WFV1 image based on Landsat OLI data and the GCPs. Moreover, the geolocation error is within one pixel. Sometimes, in the mountain areas there may exist geometrical distortion even when the relative error is within one pixel after geometric correction. However, the study area is in the central North China Plain, so the error is minimum. Therefore, the geometric correction results are reliable.

The measured spectral data were collected by the US Field Spec Pro3 ASD's field spectrometer. The effective wavelength range is from 350 to 2500 nm. The acquisition date of the measured data collected between 10:00 am and 14:30 pm is during August 19–24, 2014, in this area (summer of mid-latitude area). The weather condition was sunny with haze on that day, and the sampling locations are indicated by the yellow dots in Fig. 1. The spectral irradiance may vary significantly according to different atmospheric conditions, date, time of the day, etc. Hence, the spectral irradiance should be converted to target reflectance with a calibrated white panel, which is a useful way to minimize the errors caused by various atmospheric conditions and sun inclination. The reflectance of the object is obtained from the measured data (Eq. 2).

$$\rho_R = DN_L/DN_W * \rho_W \quad (2)$$

where ρ_R is the object reflectance. DN_L and DN_w are the DN values of object and white panel, respectively. ρ_W is the reflectance of white panel, and the value is set to be 98%.

Methodology

In this paper, we present a comparative study of atmospheric correction methods on GF-1 data, the details including models use and setting of experiment parameters of atmospheric correction models.

6S Model and Setting of Experiment Parameters

In 1997, Vermote et al. (1997) developed 6S model based on 5S model (Tanré et al. 1990). It considers the atmospheric effects of the entire radiative transfer process (sun—target-atmosphere-sensor path), and can better eliminate the influence of Rayleigh scattering and aerosols, which has been widely used in applications (Ghulam et al. 2004).

In this paper, the required parameters are provided as follows. Sun zenith is 63.6212°, sun azimuth is 136.523°, satellite zenith angle is 49.5936°, satellite azimuth is 98.9485°, and the altitude is 0.07 km. The atmospheric mode is the mid-latitude summer type. The aerosol type is continental aerosols. The satellite orbit height is 645 km. Using the parameters above, reflectance of the satellite image can be calculated by Eqs. (3) and (4)

$$y = x_a * L_\lambda - x_b \quad (3)$$

$$\rho = y/(1 + x_c * y) \quad (4)$$

where x_a, x_b and x_c are the model outputs shown in Table 2. L_λ is radiance image, and ρ is reflectance.

Table 2 Atmospheric correction parameters of each band in GF-1 WFV1 data

	Band 1	Band 2	Band 3	Band 4
x_a	0.00698	0.00697	0.00723	0.00948
x_b	0.46115	0.30598	0.17258	0.09086
x_c	0.21101	0.1662	0.12495	0.08752

FLAASH Model and Setting of Experiment Parameters

FLAASH, which developed from MOTRAN4 radiative transfer model, is a pixel-level atmospheric correction method. It can correct cascade effect caused by diffuse reflection, and is an excellent atmospheric correction method (Cooley et al. 2002). FLAASH can be used for atmospheric correction of Landsat, SPOT, WorldView, AVIRIS, Hyperion, HJ-1A/1B CCD, and other multi-spectral and hyper-spectral data (Felde et al. 2003). FLAASH model in ENVI5.2 software was used in this study. The satellite altitude is 645 km, spatial resolution is 16 m, atmospheric visibility setting is the same as the 6S model, altitude is 0.07 km, and the aerosol type selection is rural. Then, the output file is the expected reflectance.

QUAC Model and Setting of Experiment Parameters

QUAC model does not rely on complete atmospheric parameter information and directly obtains atmospheric correction parameters within the data (Bernstein et al. 2005). Based on the empirical basis of the model, it takes the mean reflectance of field view of different substances' end members to achieve atmospheric correction:

$$\rho' = (\rho_1 + \rho_2 + \rho_3 + \cdots \rho_n)/n \quad (5)$$

where ρ' is reflectance, and n is the number of the end members. QUAC model in ENVI5.2 software is used in this study.

COST Model and Setting of Experiment Parameters

COST model was developed based on DOS atmospheric correction model by Chavez (1996). It has two assumptions: (1) the minimum radiance is influenced by the scattering of atmospheric molecules, aerosols and blackbody radiation under the uniform atmospheric condition, (2) each band of the sensor offers about 1% of blackbody radiation. The COST model is described as follows.

$$\rho = \pi * D^2 * (L_\lambda - L_{haze_\lambda})/ESUN_\lambda * \cos^2(\theta) \quad (6)$$

where ρ is reflectance after atmospheric correction; D is the Sun-Earth distance, which is one astronomical unit with value of 1.5×10^{11} m; L_λ is the radiance of each band after radiometric calibration; L_{haze_λ} is the radiance of each band; $ESUN_\lambda$ is the mean solar spectral irradiance of each band at the top of the atmosphere.

ATCOR2 Model and Setting of Experiment Parameters

ATCOR2 was proposed by Richter (1990). It is a rapid atmospheric correction algorithm based on MOTRAN4, and has been widely validated and used (Manakos et al. 2011). ATCOR2, which is implemented in PCI and ERDAS, is an atmospheric correction method that removes the spectral influence caused by surface effect for the portion of the image and the clouds. Reflectance is calculated by the model with required parameters, such as date, mean elevation, center coordinates of the scene, mid-latitude summer atmospheric, and rural aerosol type.

Results

Here, we compare the results obtained from five atmospheric correction models against the TOA data. After the required parameters are inputted into the models, the atmospheric correction results are compared qualitatively and quantitatively.

Qualitative Analysis of the Atmospheric Correction Results

The composite false color image using bands 4, 3 and 2 of TOA reflectance from the original data and the results obtained from the atmospheric correction methods are shown in Fig. 2. We can see that the southeastern region of the study area is severely affected by haze with large areas of ambiguity, and the visibility of residential areas and roads affected by haze is relatively low. After atmospheric correction using 6S, FLAASH, QUAC, and COST models, there is almost no change in the sharpness of image; the haze is still there, and with the naked eye the image looked almost unchanged. The terrain object does not seem to be more clear. Main roads of the city and the residential area become clear. Compared to the results of FLAASH, QUAC, COST, and 6S, the result of ATCOR2 significantly improves the image clarity. What is more, ATCOR2 removes the haze make the blurred feature now stands out. The tiny roads effected by haze become clear. The haze effect is removed from the whole study area.

Quantitative Analysis of the Atmospheric Correction Results

Compare Measured and Model-Derived Area Mean Reflectance Before and After Atmospheric Correction

To further compare these methods, we perform qualitative assessment here, by obtaining maximum, mean and minimum values from each atmospheric correction method with those in situ measured data.

Figure 3 shows the spectrum obtained from the measured data and the mean values derived from atmospheric correction models over the observation sites. The black dashed line, the blue dotted line and the red solid line are the maximum, minimum and mean values of the in situ

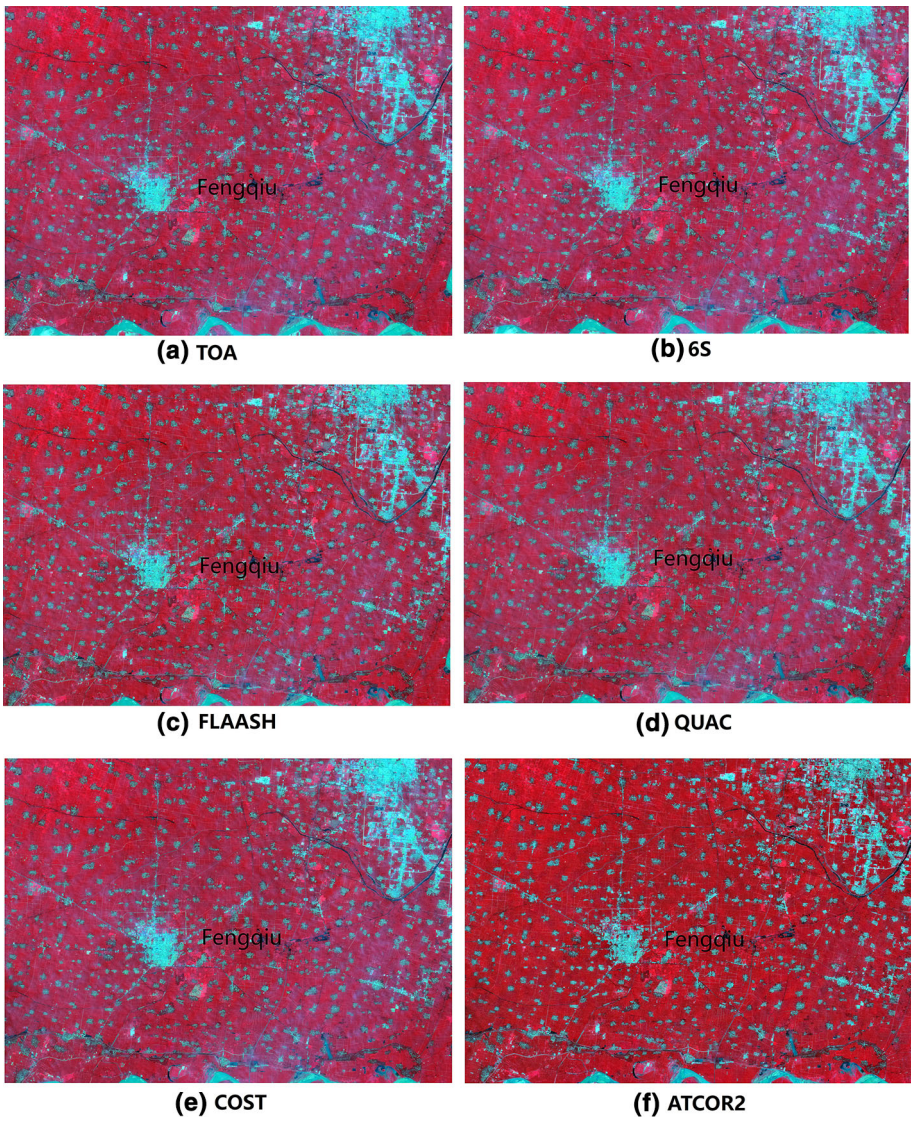

Fig. 2 A comparison of false color composite images with or without atmospheric correction

measured data. Table 3 shows the relative errors of mean values between the in situ observations and derived values. From Fig. 3, we can see that before atmospheric correction, the mean value of TOA in the first (blue) band is much greater than the second (green) and third (red) bands, smaller than the fourth band (near infrared). Compared with the in situ measured data, the TOA value of each band is higher than even the in situ measured maximum.

After atmospheric correction, the mean values of visible bands (bands 1, 2 and 3) are decreased significantly. Compared to the values of bands 1, 2, and 3 without atmospheric correction, the influence of atmospheric and haze is removed to various degrees. Compared to TOA and the mean values of the measured data, these results of atmospheric correction methods all have good performance in terms of removing atmospheric and haze effects. Specifically, the results of each model have some differences with the measured values for each band. The main reason is that the different models based on different radiative transfer patterns or methods will give different results. In addition, almost all the mean values of atmospheric correction methods are between the maximum and minimum in situ measured. In particular, ATCOR2, QUAC, and COST have the smallest differences with the mean value of in situ measured, especially in band 2 and band 3.

At band 1 (485 nm band) of Table 3, the relative error corresponding to the measured site is 6.0769 before atmospheric correction; after the atmospheric correction, relative error value is reduced significantly (especially by the ATCOR2 model, which has the minimum difference), indicating that the atmospheric correction methods achieved excellent results. At band 2 (555 nm band), the atmospheric effect is reduced to varying degrees; the relative error was reduced from 1.4046 to 0.5261-0.0647. ATCOR2 and FLAASH have the minimum relative errors.

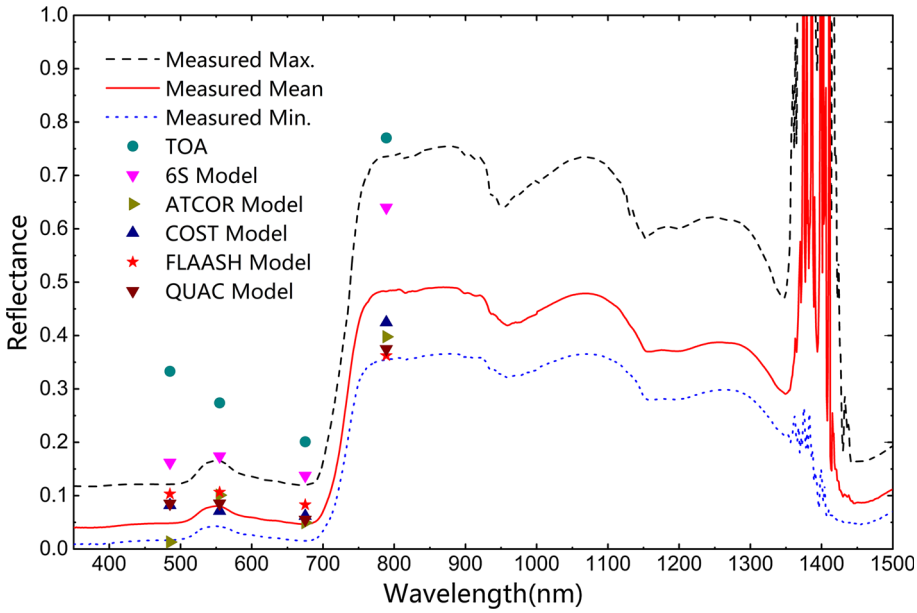

Fig. 3 The spectrum of observed values and the mean of values derived from atmospheric correction models over observation sites

Table 3 Relative error of mean values between measured values and model derived

Center wavelength	TOA-Measured	6S-Measured	ATCOR2-Measured	COST-Measured	FLAASH-Measured	QUAC-Measured
485 nm	6.0769	2.4472	0.7194	0.7433	1.1959	0.8128
555 nm	1.4046	0.5261	0.1126	0.3752	0.0647	0.2473
675 nm	2.9701	1.7192	0.0265	0.2235	0.6388	0.0899
789 nm	0.0187	0.1812	0.3901	0.3490	0.4445	0.4251
NDVI	0.3907	0.2782	0.0863	0.1273	0.2679	0.1292

At band 3 (675 nm band), the relative error is reduced from 2.9701 to 1.7192–0.02, and ATCOR2 has the minimum relative error. Band ratio can further eliminate the atmospheric influence. The relative error of NDVI decreased from 0.3900 to 0.2782–0.0863 after atmospheric correction, indicating the atmospheric effect is removed to some extent. Especially, ATCOR2 has the best agreement and minimum difference with the in situ measured NDVI.

Figure 3 and Table 3 show that the atmospheric effect is removed to a large extent by each of the models. The distribution trend of the GF-1 WFV1 spectrum data is similar to the shape of spectrum obtained from the measured data. All in all, ATCOR2 has the best performance with the minimum difference and relative error with respect to the in situ data, followed by COST and QUAC models.

Correlation Analysis Between Object Reflectance After Atmospheric Correction and the Measured Object Reflectance

To further investigate the quantitative characterization between individual and measured samples in details, the correlation coefficients between two samples are obtained. There are 178 numerical sites (N = 178) as shown in Fig. 4. Before atmospheric correction, the correlation coefficient value R^2 is 0.710 (standard deviation SD is 0.170), and R^2 increases to about 0.850 (SD to about 0.1) after atmospheric correction. ATCOR2 shows the best performance with the highest R^2 of 0.886 (SD of 0.085), followed by FLAASH model (R^2 is 0.847, SD is 0.107), QUAC (R^2 is 0.844, SD is 0.107), COST (R^2 is 0.844, SD is 0.108), and 6S (R^2 is 0.843, SD is 0.108).

Comparative Analysis of NDVI

To further evaluate the results before and after atmospheric correction, the absolute value of NDVI is calculated from model outputs, and compared with absolute value of measured NDVI. Figure 5 is the comparison between measured and model-derived NDVI. TOA-NDVI is the NDVI value calculated at TOA, which means the values were generated without atmospheric correction. 6S-NDVI, COST-NDVI, FLAASH-NDVI, QUAC-NDVI, and ATCOR2-NDVI are NDVI calculated using the 6S, COST, FLAASH, QUAC, and ATCOR2 atmospheric correction models, respectively. Measured-NDVI is the NDVI calculated by in situ measured data. As shown in Fig. 5, before atmospheric correction, TOA-NDVI has the lowest NDVI value. After atmospheric correction, five kinds of

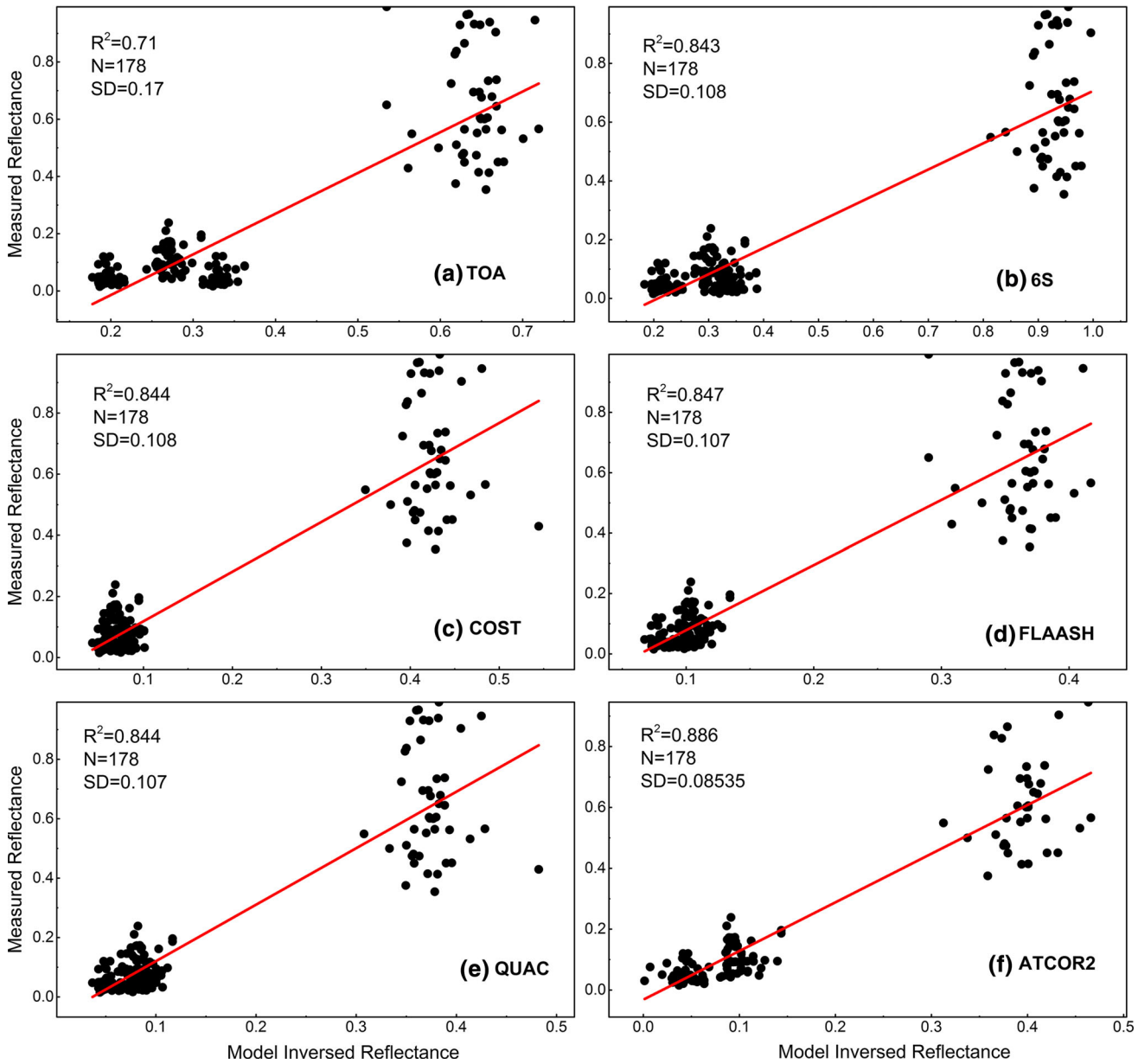

Fig. 4 Comparison between the values derived by atmospheric correction models and the measured ones

atmospheric correction methods eliminate the influence of atmosphere and haze largely compared with TOA-NDVI. The descending order of the accuracy of NDVIs is ATCOR2, COST/QUAC, 6S, and FLAASH, namely, ATCOR2 outperforms the rest (COST, QUAC, 6S, and FLAASH). The main reason is that the ATCOR2 model which has easy mathematics mode and definite physical meaning was more appropriate for use on the hazy condition. In addition, NDVI is a vegetation index calculated by near-infrared and red bands,

$$NDVI = (\rho_{NIR} - \rho_R)/(\rho_{NIR} + \rho_R) \quad (7)$$

where ρ_{NIR} is the reflectance in the NIR band, and ρ_R is the reflectance in the red band.

The longer the wavelength, the less affected by atmospheric conditions. It can be found in Figs. 2 and 3, compared with the other models, only ATCOR2 totally removes the effect of haze in green (band 2), red (band 3) and near-infrared band (band 4). Hence, ATCOR2 has the highest accuracy and minimum error.

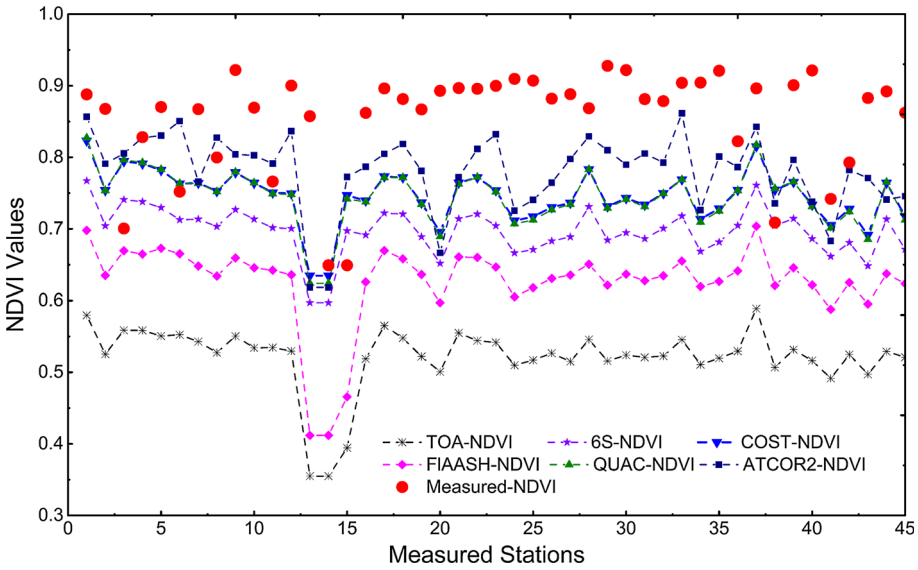

Fig. 5 Comparison between measured and derived NDVI by different atmospheric correction models

Spatial Distribution of the Absolute Error Between Derived and Measured NDVI

The spatial distribution of absolute error between derived and measured NDVI is a useful way to further assessment the atmospheric correction results. Because ATCOR2 derived data and NDVI has the highest accuracy and minimum error with the in situ measured data, absolute errors of NDVI between ATCOR2 and other models are presented in Fig. 6 to show error distribution of different atmospheric correction methods. The equation for absolute error is:

$$\Delta_x = |x_0 - x| \tag{8}$$

where other atmospheric correction model-derived NDVI value is x_0 and the ATCOR2 model derived NDVI value is x. ATCOR2-6S means the absolute error value of NDVI between ATCOR2 and 6S derived NDVI values, and same for other pairs. The range in the black curve is the study area (Fengqiu County). Figure 6 shows that the NDVI absolute error between ATCOR2 and 6S is relatively large and widely distributed with values about 0.3 in most areas. The errors of the Fengqiu County and the surrounding areas of Changyuan and Xinxiang counties are relatively large, and there is a huge difference in the rural area. For ATCOR2-COST and ATCOR2-QUAC, in a small part of the eastern region of Fengqiu County and the surrounding areas of Changyuan and Xinxiang counties, there are smaller differences mainly about 0-0.2 in most of these areas; only in some parts of urban and haze-covered area, the differences reach 0.3 or greater. For ATCOR2-FLAASH, differences are about 0.2–0.3 in the entire region of Fengqiu County, the surroundings of Changyuan and Xinxiang Counties.

Discussion

In this study, we used five atmospheric correction methods of 6S, FLAASH, QUAC, COST, and ATCOR2 on GF-1 WFV1 data to qualitatively and quantitatively investigate their performances in terms of removing haze. From the qualitative analysis results, all the models achieved remarkable results after atmospheric correction; they removed atmospheric effects to varying degrees. ATCOR2 showed the best performance. The clarity of COST, FLAASH, QUAC, and 6S is slightly increased. However, it is difficult to tell the improvements of the data after atmospheric correction using these models. Quantitative analysis evaluated the following four aspects: (1) comparing the mean reflectance between measured and model derived data before and after atmospheric correction; (2) correlation analysis between object reflectance after atmospheric correction and the measured data; (3) comparative analysis of vegetation indices; and (4) spatial distributions of absolute error between two different methods. The evaluated results showed that all the methods achieved remarkable results and removed atmospheric effects in varying degrees compared with TOA. However, for (1), the trends of ATCOR2, COST and QUAC model-derived values had the most consistent agreement with the measured values, and the difference between ATCOR2 and the measured data as the smallest, followed by COST, QUAC, FLAASH and 6S models. For (2), several models showed different atmospheric correction results according to correlation coefficients; ATCOR2 had the best agreement with the measured data, followed by FLAASH, COST, QUAC, and 6S. However, the differences were not significant. For (3), the ascending order of mean differences values between the measured and derived NDVI was

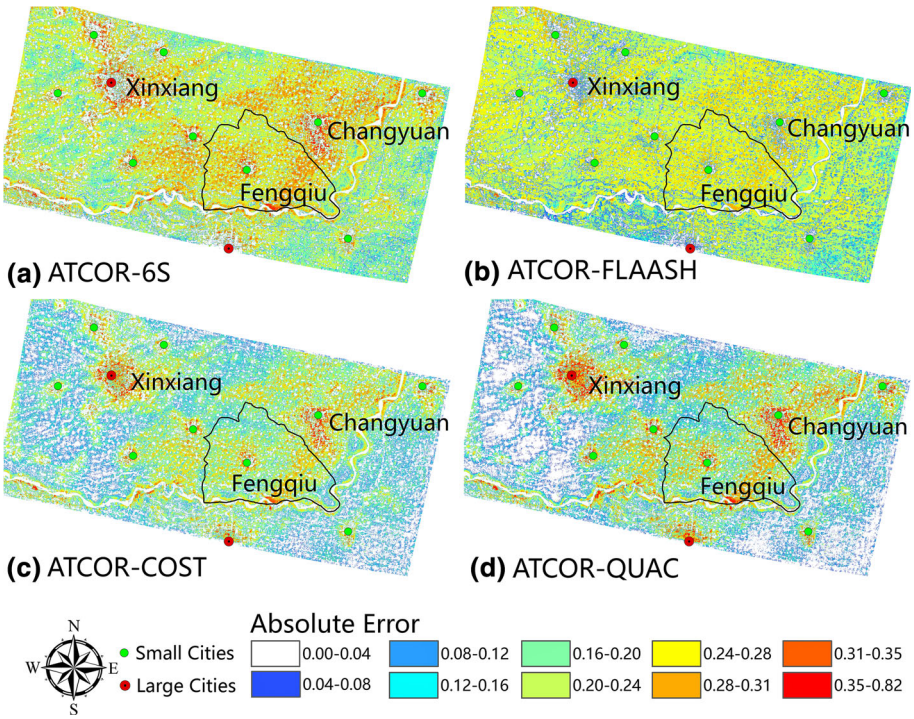

Fig. 6 Absolute error distributions of derived NDVI by different atmospheric correction methods

ATCOR2, COST, QUAC, FLAASH, and 6S. For (4), the error was mainly located in the haze-influenced area and the peri-urban area. Overall, these indicate that the descending order of the capability during hazy is ATCOR2, COST, QUAC and FLAASH, 6S in the study area.

Usually, physically based absolute atmospheric correction methods are better than statistically or empirically based relative atmospheric correction model. However, we found that the results of QUAC and COST methods are better than 6S and FLAASH methods under hazy in this study. This may be because the relative atmospheric correction relies on the assumption that the relation between the radiance of TOA and ground follows a linear trend for the various terrain objects in an image. Though this linear relationship is an approximation to the real situation in fact, it is accurate enough to solve some practical applications, especially when there are other main sources of errors that may influence the results and little information is known about the ground. For the absolute atmospheric correction, if adequate atmospheric profiling parameters are offered, the estimation error can be controlled within 10%. Unfortunately, enough atmospheric profiling required for these methods is rarely available. Hazy makes atmospheric profiling more complex, which makes it worse for atmospheric correction of the GF-1 WFV1 data. This may be the reason why the physically based FLAASH and 6S performed not as well as the statistically or empirically based COST and QUAC.

As mentioned earlier, the ATCOR2 model has the best performance qualitatively and the best agreement with the in situ measured data quantitatively in terms of removing haze. In qualitative assessments, as shown in Fig. 1, the GF-1 WFV1 data contain haze areas (white or grey area in the image), though in the hazy regions some terrain surface information can still be recognized. The GF-1 WFV1 image was divided into clear and hazy regions using the ATCOR2 method. The western part of the image is clear region, which has no white or grey haze; on the contrary, the eastern part especially the area around Fengqiu County is hazy region. The clear and hazy regions can be seen in Figs. 1, 2 and 6. The previous study showed that there was a high correlation among the four bands of GF-1 WFV1 data. As the blue band with a short wavelength is easily influenced by haze (mainly via Rayleigh and Mie's scattering) than the other bands. The correlation between the blue and red bands was decreased when influenced by haze. Then, the tasseled cap transformation was used to mask the clear and hazy areas. After that, a regression relationship between the blue and red bands was calculated for the clear area, and the hazy area was orthogonal to the regression slope. Then, the histogram of hazy image can be calculated. Therefore, a functional relationship between the histogram of hazy image and a clear image was established. Using this functional relationship, we corrected the hazy image data. All of these factors made the ATCOR2 model most appropriate for removing haze of this area than the other methods. In quantitative assessments, the total signal received by the sensor consisted of path radiance, the viewing terrain object pixel radiance, radiance from adjacent pixels, and terrain radiation caused by undulating

terrain surface. The atmospheric parameters like aerosol type, transparency and water vapor, etc. can be estimated preciously using the ATCOR2 method with the SPECTRAL module.

Since the atmospheric database contains a large number of predefined transmission parameters calculated by MODTRAN-4 which can be apply for different solar elevation angles, climate conditions, etc., radiance from adjacent pixels can be calculated since the ATCOR2 model include a correction for the pixel mixing due to the radiance from adjacent pixels.

Terrain radiation caused by undulating terrain surface can be ignored since the study area is located in flat plain where ATCOR2 is mostly suitable. After the calculated what of path radiance and the radiance from adjacent pixels, the viewing terrain object pixel radiance can be calculated accurately. All of these combined with the haze-removing procedure mentioned above make ATCOR2 have the optimum performance quantitatively.

Conclusions

Five atmospheric correction methods were studied based on GF-1 WFV1 data under hazy condition. Specifically, we examined performances of these methods qualitatively in terms of removing haze, and then quantitatively in terms of correlation value, relative error, NDVI value, etc. We conclude that the ATCOR2 method takes into consideration not only the atmosphere and radiation transfer process, but also the relevant factors. Hence, after the atmospheric correction, the image becomes clearly, atmospheric and hazy effects are eliminated. We also find the spatial distributions of errors are mainly located in haze and peri-urban area with mainly complex and volatile aerosols. Since we lack useful detailed in situ measured parameters of haze and the complex, volatile optical property of haze and urban aerosols, there is a lot of work to be done in atmospheric correction under haze.

In the eastern part of China, haze shows an increasing trend, which severely limits the application of optical remote sensing data. Based on our study, the ATCOR2 model achieves better performance in eliminating atmospheric effects. Therefore, it should have a good potential for many applications under haze. In our future work, more in situ measured data such as adequate atmospheric profiling parameters and the optical properties of PM2.5 and urban aerosols should be considered with the aim of achieving more accurate atmospheric correction results.

Acknowledgements The authors would like to thank the reviewers, the editors, and Dr. Jike Chen for their highly constructive comments and remarks. The authors would like to thank China Resources Satellite Application Center for providing the GF-1 WFV1 data. This study was supported by the National Key Research and Development Program of China (2016YFC1400901), the High Resolution Earth Observation Systems of National Science and Technology Major Projects (41-Y20A31-9003-15/17), the National Science Foundation of China (41476156, 41621064), and the Public Science and Technology Research Funds Projects of Ocean (201005030).

References

Bernstein, L. S., Adler-Golden, S. M., Sundberg, R. L., Levine, R. Y., Perkins, T. C., & Berk, A., et al. (2005). *A new method for atmospheric correction and aerosol optical property retrieval for VIS-SWIR multi- and hyperspectral imaging sensors: QUAC (QUick atmospheric correction).* Paper presented at the geoscience and remote sensing symposium, 2005. IGARSS '05. Proceedings. 2005 IEEE International.

Chavez, P. S. (1988). An improved dark-object subtraction technique for atmospheric scattering correction of multispectral data. *Remote sensing of environment, 24*(3), 459–479.

Chavez, P. S. (1996). Image-based atmospheric corrections-revisited and improved. *Photogrammetric Engineering and Remote Sensing, 62*(9), 1025–1035.

Cooley, T., Anderson, G. P., Felde, G. W., Hoke, M. L., Ratkowski, A. J., & Chetwynd, J. H., et al. (2002). *FLAASH, a MODTRAN4-based atmospheric correction algorithm, its application and validation*. Paper presented at the geoscience and remote sensing symposium, 2002. IGARSS '02. 2002 IEEE International.

Felde, G. W., Anderson, G. P., Cooley, T. W., Matthew, M. W., Adler-Golden, S. M., & Berk, A., et al. (2003). Analysis of Hyperion data with the FLAASH atmospheric correction algorithm. In *IEEE international symposium on geoscience and remote sensing (IGARSS)* (pp. 90–92).

Gao, B., Montes, M. J., Davis, C. O., & Goetz, A. F. H. (2009). Atmospheric correction algorithms for hyperspectral remote sensing data of land and ocean. *Remote Sensing of Environment, 113,* S17–S24.

Ghulam, A., Qin, Q., Zhu, L., & Abdrahman, P. (2004). Satellite remote sensing of groundwater: Quantitative modelling and uncertainty reduction using 6S atmospheric simulations. *International Journal of Remote Sensing, 25*(23), 5509–5524.

Guo, H. (2014). Evaluation of four dark object atmospheric correction methods based on ZY-3 CCD Data. *Spectroscopy & Spectral Analysis, 34*(8), 2203–2207.

Guo, Y., & Zeng, F. (2012). Atmospheric correction comparison of SPOT-5 image based on model FLAASH and model QUAC. In: *ISPRS—International archives of the photogrammetry, remote sensing and spatial information sciences* (Vol. 39, No. b7, pp. 7–11).

Han, X. Q., Yi, S. U., Jing, L. I., Zhang, Y., Liu, J., & Gao, W. M. (2012). Atmospheric correction and verification of the SPOT remote sensing image in coastal zones. *Geographical Research, 31*(11), 2007–2016.

He, G., Xiao, P., Feng, X., Zhang, X., Wang, Z., & Chen, N. (2015). Extracting snow cover in mountain areas based on SAR and optical data. *IEEE Geoscience and Remote Sensing Letters, 12*(5), 1136–1140.

Karpouzli, E., & Malthus, T. (2003). The empirical line method for the atmospheric correction of IKONOS imagery. *International Journal of Remote Sensing, 24*(5), 1143–1150.

Li, Z., Mei, L. Y., Hua, Z. S., & Long, G. Y. (2015). Remote sensing monitoring of Taihu Lake water quality by using GF-1 satellite WFV data. *Remote Sensing for Land and Resources, 27*(1), 113–120.

Liang, S., Fang, H., & Chen, M. (2001). Atmospheric correction of Landsat ETM + land surface imagery. I. Methods. *IEEE Transactions on Geoscience and Remote Sensing, 39*(11), 2490–2498.

Liang, S., Fang, H., & Chen, M. (2002). Atmospheric correction of Landsat ETM + land surface imagery: II. Validation and applications. *IEEE Transactions on Geoscience & Remote Sensing, 40*(12), 1–10.

Lu, D., Mausel, P., Brondizio, E., & Moran, E. (2002). Assessment of atmospheric correction methods for Landsat TM data applicable to Amazon basin LBA research. *International Journal of Remote Sensing, 23*(13), 2651–2671.

Manakos, I., Manevski, K., & Kalaitzidis, C. (2011). Comparison between FLAASH & ATCOR atmospheric correction modules on the basis of WorldView-2 imagery and in situ spectral radiometric measurements. In *7th EARSeL SIG imaging spectroscopy workshop*.

Matthew, M. W., Adler-Golden, S. M., Berk, A., & Felde, G. (2003). Atmospheric correction of spectral imagery: Evaluation of the FLAASH algorithm with AVIRIS data. In *Aerosense* (Vol. 5093, pp. 157–163). International Society for Optics and Photonics.

Peng, N. (2008). Atmospheric correction of QuickBird-2 imagery for turbid water coastal areas using MODIS data. *Acta Optica Sinica, 28*(5), 817–821.

Richter, R. (1990). A fast atmospheric correction algorithm applied to landsat TM images. *International Journal Remote Sensing, 11*, 159–166.

Richter, R. (1996). Atmospheric correction of satellite data with haze removal including a haze/clear transition region. *Computers & Geosciences, 22*(6), 675–681.

Richter, R. (1997). Correction of atmospheric and topographic effects for high spatial resolution satellite imagery. *International Journal of Remote Sensing, 18*(5), 1099–1111.

Tanré, D., Deroo, C., Duhaut, P., Herman, M., Morcrette, J. J., Perbos, J., et al. (1990). Technical note Description of a computer code to simulate the satellite signal in the solar spectrum: The 5S code. *International Journal of Remote Sensing, 11*(4), 659–668.

Vermote, E. F., Tanre, D., Deuze, J. L., Herman, M., & Morcette, J. J. (1997). Second simulation of the satellite signal in the solar spectrum, 6S: An overview. *IEEE Transactions on Geoscience and Remote Sensing, 35*(3), 675–686.

Wang, X. F., Mao, Z. H., & Chen, J. Y. (2011). Atmospheric correction of the SPOT satellite data of the coastal zones. *Journal of Marine Sciences, 29*(1), 68–72.

Wang, Z. T., Wang, H. M., Qing, L. I., Zhao, S. H., Shen-Shen, L. I., Chen, L. F., et al. (2014). A quickly atmospheric correction method for HJ-1 CCD with deep blue algorithm. *Spectroscopy & Spectral Analysis, 34*(3), 729–734.

Wu, J., Wang, D., & Bauer, M. E. (2005). Image-based atmospheric correction of QuickBird imagery of Minnesota cropland. *Remote Sensing of Environment, 99*(3), 315–325.

Wu, M., Huang, W., Zheng, N., & Wang, C. (2015). Combining HJ CCD, GF-1 WFV and MODIS data to generate daily high spatial resolution synthetic data for environmental process monitoring. *International Journal of Environmental Research & Public Health, 12*(8), 9920–9937.

Qi, X. Y., & Tian, Q. J. (2005). The advances in the study of atmospheric correction for optical remote sensing. *Remote Sensing for Land & Resources, 17*(4), 1–6.

Yang, Y. L., Zhao, N., & Cheng, X. Q. (2015). Atmospheric correction and evaluation of SPOT6 satellite image based on FLAASH model. *Modern Surveying & Mapping*, (2), 3–6.

Yao, W., Li, Z. J., Yao, G., Wu, J. F., & Jiang, D. L. (2011). Atmospheric correction model for Landsat images. *Transactions of Atmospheric Sciences, 34*(2):251–256.